



ELSEVIER

Surface Science 344 (1995) 111–121

surface science

Structural evolution during electrocrystallization: deposition of Tl on Ag(100) from monolayer to bilayer and to bulk crystallites

J.X. Wang^{a,*}, R.R. Adžić^a, O.M. Magnussen^b, B.M. Ocko^b

^a Department of Applied Science, Chemical Sciences Division, Brookhaven National Laboratory, Upton, NY 11973, USA

^b Department of Physics, Brookhaven National Laboratory, Upton, NY 11973, USA

Received 12 May 1995; accepted for publication 20 July 1995

Abstract

The structure of Tl overlayers deposited at underpotentials and the structure of bulk deposited Tl on Ag(100) in perchloric acid have been determined using surface X-ray scattering. Thallium forms a $c(p \times 2)$ close-packed monolayer which compresses uniaxially (p decreasing from 1.185 to 1.168) with decreasing potential. Upon deposition of the second layer, the first layer expands slightly along the incommensurate direction and both layers form a $c(1.2 \times 2)$ structure. Bulk deposition at potentials negative of the Nernst potential results in the formation of well aligned hcp Tl crystallites atop the $c(1.2 \times 2)$ bilayer. The stability of the bilayer structure in the presence of bulk deposits and its pronounced effects on subsequent epitaxial growth are discussed in terms of strain and interface energies.

Keywords: Electrochemical methods; Epitaxy; Surface structure; Thallium; X-ray scattering

1. Introduction

In heteroepitaxy, the structure of the first one or two deposited layers often differs from the bulk phase. When the lattice mismatch between the bulk structure of the deposits and the substrate is small, monolayers form commensurate or uniaxially commensurate structures to reduce the lattice mismatch and consequently the interface energy. This often requires a lattice distortion from the bulk structure of the deposit [1–3]. In the case that the lattice mismatch is large and that the adatom is larger than the substrate atom, incommensurate or disordered phases usually form depending upon the substrate corrugation. On hexagonally close-

packed substrate surfaces many incommensurate hexagonal monolayers have been observed [4–10]. The incommensurate monolayers align with the substrate in a defined direction in order to minimize the interface energy. In addition, they often have different layer densities compared to their bulk values and this is a consequence of the reduced coordination at the surface and the interaction with a dissimilar substrate material. Thus, ordered monolayers are strained with respect to the bulk from the combined effects (mismatch, coordination, substrate) discussed above [11].

With increasing thickness, the substrate effect decreases as the distance from the substrate to the n th overlayer increases; hence, the in-plane structure of the n th overlayer tends to become more and more bulk-like. The underlying overlayers may restructure due to the additional interaction with

* Corresponding author. Fax: +1 516 282 3137; E-mail: jia@solids.phy.bnl.gov.

the overlayers above it. Therefore, the structure evolution during heteroepitaxial growth can be rather complex. Considerable attention has been devoted to this topic because of its importance in ultrathin film studies and the pronounced effects of initial adlayer structures on the crystalline perfection and the in-plane orientation of the bulk deposits [5,12,13].

At hexagonally close-packed metal-metal interfaces, the in-plane lattice strains of the initial overlayer(s) are often relaxed by a restructuring of the respective layer(s). As shown recently for Cu on Ru(0001), the in-plane structure of the Cu overlayer(s) change from pseudomorphic (i.e. 1×1 commensurate), to uniaxially incommensurate and to incommensurate structures with increasing film thickness [13]. At each structural transition, all the underlying layers seem to rearrange to a structure which is more bulk-like and less commensurate with the substrate. A similar phenomenon has been observed using SXS for electrodeposition of Pb on Ag(111) [5]. The underpotentially deposited (UPD) Pb forms an incommensurate hexagonal monolayer with a layer density 6% higher than the bulk value prior to bulk deposition. The compressed Pb monolayer restructures after overpotential deposition of 5 nominal atomic layers and the bulk lead grows as islands which have the (111) texture of its fcc bulk crystal but are randomly oriented in the plane of the Ag(111) substrate. These results suggest that creating an additional interface between the initial adlayer and the less strained new layers often requires more energy than that needed for restructuring the initial adlayer(s) at hexagonal close-packed surfaces.

In contrast, results for the electrodeposition of Tl on Au(100) have shown that the uniaxially-commensurate monolayer is stable under the bulk deposits which have a hcp structure, predominately aligned along the substrate axes [3]. It appears that the increased substrate corrugation (the (100) surface is more corrugated than the (111) surface) stabilizes the uniaxially incommensurate monolayer against the restructuring to the bulk-like bidirectionally incommensurate structure. This, in turn significantly improves the ordering of bulk deposits. To investigate the role of the substrate corrugation and to study the effect of the substrate

interaction strength on the interface structure, SXS measurements were carried out for the electrodeposition of Tl on Ag(100). The latter is feasible since Ag(100) has nearly identical lattice constants as Au(100), but a different work function. In this paper, results of SXS measurements for Tl/Ag(100) are reported and compared with those for Tl/Au(100).

Previous voltammetric investigations have suggested that UPD of Tl on Ag(100) consists of three distinct potential regions [14]. Based on the assumptions made for the three current peaks, a commensurate monolayer, bilayer, and trilayer with a $1/2$ coverage in each layer have been proposed in the different potential regions. Direct structural studies on this system have not been reported up to now although Pb/Ag(111),(100) and Tl/Ag(111) have been extensively studied as prototypical systems for UPD and electrocrystallization [10,15]. Our SXS data show that the first broad cathodic current peak corresponds to submonolayer adsorption in a disordered phase which is followed by the second current peak leading to the formation of a uniaxially commensurate monolayer. Prior to bulk deposition, the second Tl overlayer is deposited which causes a restructuring of the first layer. The bilayer structure is stable, even after bulk deposition. As a high resolution and three-dimensional structural probe, SXS provides accurate in-plane lattice parameters and clear identifications of the mono-, bi-, and multi-layer nature of each phase during the growth. On the basis of these detailed structural studies and comparisons with other systems, the important factors which control the evolution of interface structure in heteroepitaxy are identified.

2. Experimental

The Ag(100) single crystal, oriented within 0.2° from the $\langle 100 \rangle$ crystallographic plane, was chemically polished using $\text{Cr}_2\text{O}_3/\text{HCl}$ solution [16]. The sample was then transferred with a drop of water covering the surface into an electrochemical X-ray scattering cell constructed from Kel-F [17]. The cell was sealed using a $4 \mu\text{m}$ thick Prolene (Chemplex Inc.) X-ray window. The solutions

were prepared from Ti_2SO_4 (Johnson Matthey, 99.99 + %), HClO_4 (Merck, Suprapur) and Milli-Q water (Millipore Inc.). Since underpotential deposited Tl overlayers are not stable in the presence of oxygen, an outer cell was filled with high purity nitrogen gas to keep the solution free of oxygen during the measurements. The cell can be inflated to have 2–4 mm thick solution above the crystal surface and deflated for X-ray measurements with a thin ($\sim 10 \mu\text{m}$ thick) capillary electrolyte film between the Ag(100) face and the X-ray window. A reversible hydrogen electrode in 0.1M HClO_4 was used as a reference electrode. All potentials are cited with respect to normal hydrogen electrode (NHE).

SXS measurements were carried out at the National Synchrotron Light Source (NSLS) at beam line X22B with $\lambda = 1.54 \text{ \AA}$. A full description of the electrochemical SXS technique has been presented elsewhere [17]. For in-plane diffraction measurements, the q -space resolution within the scattering plane was determined primarily by a 1 mrad Soller slit on the detector arm. For measurements of integrated intensity, a 2 mm wide slit was used in the scattering plane which has an acceptance of 3 mrad. The transverse in-plane resolution was limited by the mosaic spread of the silver single crystal which is about 0.1° half width at half maximum (HWHM). For convenience, the unit cell for Ag(100) surface is chosen to have one silver atom per unit cell within the plane, i.e., with two lattice vectors pointing to in-plane nearest neighbor Ag atoms (length $a = 2.889 \text{ \AA}$) and the third vector, c (4.086 \AA), along the surface normal. A position in reciprocal space in this coordinate system is given by $(a^*, b^*, c^*) \cdot (H, K, L)$, where $a^* = b^* = 2\pi/a = 2.175 \text{ \AA}^{-1}$, and $c^* = 2\pi/\sqrt{2}a = 1.538 \text{ \AA}^{-1}$. The in-plane diffraction measurements were carried out in the (H, K) plane at $L = 0.1$, corresponding to a grazing incident angle of 1.1° .

3. Results and discussion

3.1. Voltammetry

The linear potential sweep voltammetry curve for the UPD of Tl on Ag(100) in 0.1M HClO_4

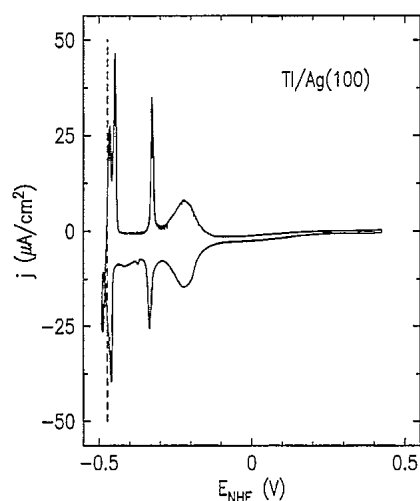


Fig. 1. Linear sweep voltammogram for UPD of Tl on Ag(100) in 0.1M HClO_4 with 2.5mM Ti_2SO_4 obtained in a conventional electrochemical cell. The Nernst potential for Tl bulk deposition is indicated by the dashed line. Sweep rate 5 mV/s.

containing 2.5mM Ti_2SO_4 is shown in Fig. 1. The basic features are the same as that previously reported [14]. The broad cathodic peak at -0.225 V shows the initial UPD of Tl. It is followed by the sharp peak at -0.335 V which, according to our SXS measurements, corresponds to the formation of a close-packed Tl monolayer. At -0.460 V , the large peak signals the deposition of the second Tl layer which occurs at a potential about 10 mV positive of the bulk deposition. Below the reversible Nernst potential of -0.472 V (dashed line), the onset of bulk deposition gives rise to a sharp increase of the cathodic current. Upon reversing the sweep direction the cathodic current decreases which is followed by a bulk stripping peak at -0.47 V . It should be noted that close to the reversal point the current in the positive going sweep exceeds that of the sweep in negative direction. This so called “nucleation loop” is a well-known phenomenon in bulk deposition related to a kinetic hindrance of the nucleation of the metal deposit. Relative to the deposition process, the stripping of the bilayer and the monolayer in the anodic sweep proceeds in a nearly reversible manner. The charges associated with the anodic peaks at -0.465 , -0.327 , and -0.225 V are about 135, 80, and $95 \mu\text{C}/\text{cm}^2$, respectively. Assuming a one-electron exchange in the UPD of Tl, this is

equivalent to 0.7, 0.4, and 0.5 of a monolayer, since for Ag(100) a monolayer coverage requires $191 \mu\text{C}/\text{cm}^2$. From our SXS measurements discussed in the following subsections, the actual Tl coverage in the bilayer phase is $0.833 \times 2 = 1.67$ and in the monolayer phase ranges from 0.856 to 0.844 in the potential region between -0.46 and -0.32 V. Since the total charge associated with the three stripping peaks is equivalent to 1.6 of a monolayer, the dissolution of Tl appears to be completed at -0.1 V.

3.2. Monolayer structure

Grazing incident angle X-ray diffraction measurements were carried out to determine the Tl monolayer structure on Ag(100) at potentials positive of -0.46 V in 0.1M HClO_4 solution containing 2.5mM Tl_2SO_4 . Fig. 2a shows the in-plane diffraction pattern observed at -0.44 V. Besides the reflections from the Ag(100) substrate which are

indexed by the integers, additional reflections (open circles) were observed indicating that the Tl adlayer develops long range order at this potential. The non-integer reflections exhibit a centered rectangular symmetry i.e., all the diffractions are found at $(m\delta, n/2)$ when the sum of m and n is even. The corresponding real space model is given in Fig. 2b and shows the $c(p \times 2)$ symmetry, where $p = 1/\delta$, and the quasi-hexagonal packing of the Tl adatoms. The HWHM of the diffraction peak at $(\delta, 0.5)$ is 0.005 \AA^{-1} along both H and K directions. The lower bound on the coherence length (i.e., the average domain size) is thus $1/\text{HWHM} = 200 \text{ \AA}$ along both incommensurate direction (H) and commensurate (K) directions.

The $c(p \times 2)$ phase was found to be uniaxially compressible with potential along the incommensurate direction. Representative diffraction profiles along H at $K = 1/2$ at several potentials are displayed in Fig. 2c, which are well described by a Lorentzian line shape as shown by the solid lines. Superstructure peaks are observed up to -0.32 V, where the diffracted intensity decreases sharply due to the phase transition corresponding to the second anodic current peak in the voltammogram. Within the potential region between -0.46 and -0.32 V, the shift of the diffraction peak with increasing potential demonstrates the uniaxial expansion of the Tl lattice. Since the area per Tl adatom is $2a \times pa/2 = pa^2$, the Tl coverage in terms of the number of Tl per Ag is equal to $a^2/(pa^2) = \delta$. This can be directly measured from the peak position. Fig. 3a displays the Tl coverage as a function of potential in the $c(p \times 2)$ phase. The data were taken in an anodic (dissolution) and a cathodic (deposition) potential scan in 20 mV steps. At each potential, the diffraction measurement takes 2 min. Inflating the cell or waiting a long time after a step change of potential does not significantly affect the data obtained during the anodic scan, but does slightly increase the coverage in the cathodic scan. These effects can be explained by the transport properties of the thin electrolyte layer on top of the Ag sample. The deposition of additional Tl atoms during the cathodic scan requires transport of Tl from the solution to the interface. In our experiments this process is kinetically hindered by the thin layer geometry. In contrast, the desorption

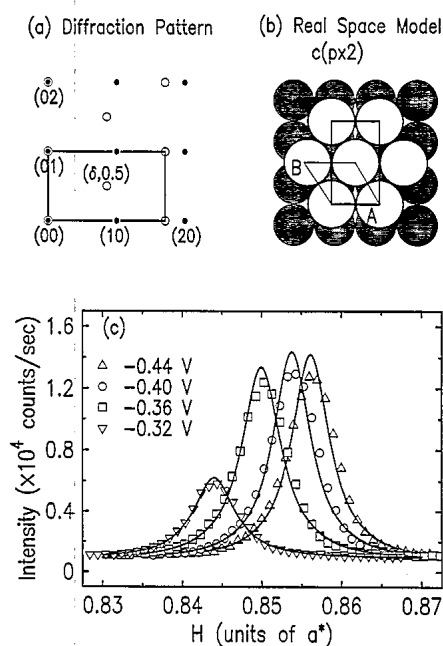


Fig. 2. (a) In-plane diffraction patterns for the Tl $c(p \times 2)$ monolayer (open circles) on Ag(100) (solid circles). For clarity, only one of the two symmetry equivalent domains of the $c(p \times 2)$ phase is shown. (b) Real space model deduced from the observed diffraction pattern shown in (a). (c) Diffraction intensity profiles along the H direction through the $(\delta, 0.5)$ position at different potentials in 0.1M HClO_4 with 2.5mM Tl_2SO_4 . The solid lines are the fits to the Lorentzian line shape.

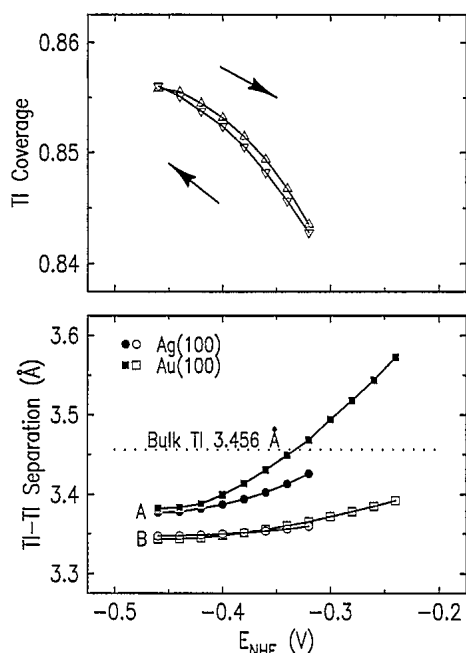


Fig. 3. (a) Tl coverage on Ag(100) and (b) Tl-Tl separations in the $c(p \times 2)$ phase on Ag(100) and Au(100) as a function of potential in 0.1M HClO_4 with 5mM Tl^+ . In (b), the data were obtained in an anodic scan and the filled and open circles (squares) are the Tl-Tl separations of "A" and "B" (cf. Fig. 2b) on Ag(100) (Au(100)), respectively.

of Tl during the anodic scan is largely not affected by transport processes and therefore close to equilibrium. This difference is the main cause of the small differences in coverage between the two curves shown in Fig. 3a.

A comparison of the in-plane near neighbor separations in the $c(p \times 2)$ Tl monolayer on Ag(100) with that on Au(100) is shown in Fig. 3b. The Tl-Tl separation between the atoms in the incommensurate direction ($A = pa$, see Fig. 2b) is slightly larger than the one between the atoms in two adjacent rows ($B = \sqrt{(1 + p^2/4)}a$). Note that the substrate lattice constant, a equals to 2.889 and 2.884 for Ag(100) and Au(100), respectively. The minimum Tl-Tl separation on Ag(100) at the most negative potential is nearly the same as that on Au(100) as well as that in the hexagonal Tl monolayer on Ag(111) [6] and Au(111) [7]. This is probably due to the steeply increasing repulsive interaction between the adatoms which dominates the adlayer structure at small separations. Hence, the maximum compression is not sensitive to the

substrate interaction. At other potentials, the Tl spacings increase faster on Au(100) with increasing potential than on Ag(100). More significantly, the $c(p \times 2)$ phase vanishes at different potentials and with different Tl spacings on the two surfaces. On Au(100), the anodic current associated with the phase transition is very small indicating only small changes of the Tl coverage [3]. Apparently, the adlayer disorders if the lattice spacing exceeds a critical value, which is determined by the lateral interactions. In contrast, on Ag(100) the weaker substrate-adatom interaction of Tl on Ag than on Au [18] causes dissolution of substantial amounts of Tl at about -0.33 V (cf. Fig. 1) preventing further expansion of the $c(p \times 2)$ phase.

Following the sharp anodic current peak at -0.33 V, a broad current peak occurs over a 0.2 V potential region (cf. Fig. 1). The latter suggests a more rapid (as compared to the $c(p \times 2)$ phase) and continuous desorption of the Tl submonolayer which usually implies that the submonolayer is disordered. We limited our search for ordered submonolayers to a few commensurate structures. No diffraction was found at (0.5, 0.5) over the potential region from -0.4 to 0 V. This rules out the existence of $c(2 \times 2)$, $c(2\sqrt{2} \times \sqrt{2})$, and (2×2) phases.

3.3. Bilayer structure

As discussed in the previous subsection, the diffraction peak at $(\delta, 0.5)$ from the $c(p \times 2)$ Tl monolayer shifts to larger δ with decreasing potential corresponding to a continuous increase of Tl coverage. Saturation is attained at -0.46 V with $\delta = 0.856$. Decreasing the potential further to -0.47 V, where the cathodic current increases sharply, results in a decrease of diffracted intensity at $(0.856, 0.5)$. The cell was inflated at this potential for several minutes to ensure that deposition is not kinetically hindered by the thin film geometry. In the subsequent in-plane diffraction measurements, the $(0.856, 0.5)$ and $(1.702, 0)$ peaks vanished and more intense peaks were found at $(0.833, 0.5)$ and $(1.667, 0)$, as shown in Fig. 4. Further decrease of potential has no effect on the peak position. Based on these observations, a commensurate $c(1.2 \times 2)$

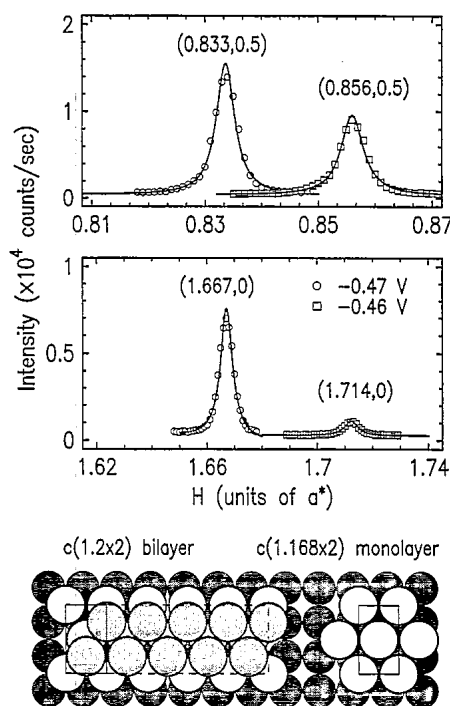


Fig. 4. Upper panels: diffraction scans along the H direction through two low-order diffractions of the $c(1.2 \times 2)$ Tl bilayer (circles) at -0.47 V and of the $c(p \times 2)$ monolayer (squares) at -0.46 V. The solid lines are the fits to a Lorentzian line shape. Lower panel: the real space models for the commensurate $c(1.2 \times 2)$ bilayer and the $c(p \times 2)$ monolayer. The diameter ratio of the open (the first Tl layer) and lightly shaded (the second Tl layer) circles to the filled (Ag) circles is $3.456/2.889 = 1.196$, which equals to the ratio of bulk Tl separation in the hexagonal plane (3.456 Å) over the Ag–Ag separation (2.889 Å).

bilayer structure is proposed. As shown in the bottom panel of Fig. 4, there are ten Tl atoms in a 6×2 unit cell in each layer. The first Tl layer undergoes a uniaxial expansion from $p = 1.168$ to 1.2 and becomes commensurate with the substrate, the second Tl layer is pseudomorphic with the first one. The coherence length of this bilayer is about 300 Å which is similar to the substrate facet size, but larger than that of the uniaxially commensurate $c(p \times 2)$ monolayer.

Direct proof that this structure corresponds to a Tl bilayer rather than a different monolayer phase is obtained from the oscillations observed in the surface rods, i.e. the L dependence of the diffracted intensity from laterally ordered surface layers at the $(0.833, 0.5)$ and $(1.667, 0.5)$ positions (Fig. 5). The diffracted intensity was determined

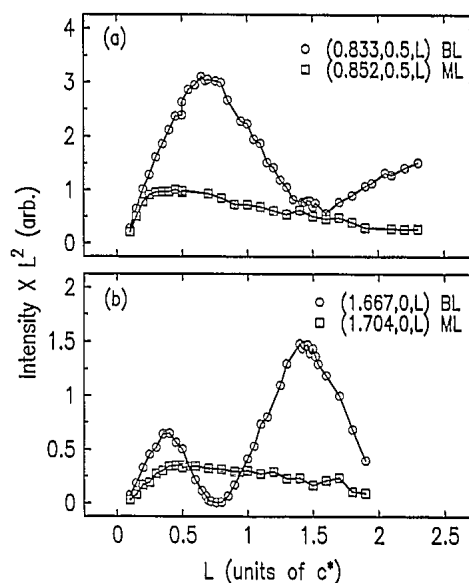


Fig. 5. Surface rods (the L dependence of diffracted intensity from ordered surface layers) measured at -0.44 V for the $c(p \times 2)$ monolayer (squares) and at -0.47 V for the $c(1.2 \times 2)$ bilayer (circles). The diffracted intensity was measured by integrating the θ rocking curve at each L and was multiplied by L^2 after correction for the X-ray polarization.

by integrating the θ rocking curve at each L and then multiplying by L^2 after correcting for the X-ray polarization. The data obtained at $(0.852, 0.5)$ and $(1.704, 0)$ positions at -0.44 V show no oscillation with L , as expected for a two-dimensionally ordered monolayer which has no periodic structure along the surface normal direction. On the other hand, the surface rods obtained at -0.47 V (circles) oscillate with a period of about $1.48c^*$ resulting from the interference between the two $c(1.2 \times 2)$ Tl layers. The diffracted intensity decreases at small L for all the rods because the absorption in the thin solution layer becomes strong at these small incident angles. Therefore, the estimated oscillation period of $1.48c^*$ is obtained using the minimum and maximum at large L in the $(0.833, 0.5)$ and $(1.667, 0)$ rods, respectively. The layer spacing between the two Tl layers can be calculated from $4.086/1.48 = 2.76$ Å which is very close to the layer spacing of 2.763 Å in hcp Tl bulk crystal.

The formation of a bilayer composed of two mutually commensurate layers has also been observed in the UPD of Tl on Ag(111) where both

monolayer and bilayer have an incommensurate hexagonal lattice rotated a few degree from the substrate axes [6]. Upon bilayer formation the layer density, relative to hcp bulk Tl, changes from 1.062 to 1.035 on Ag(111) and 1.061 to 1.033 on Ag(100) (cf. Fig. 8a), i.e., by nearly the same amount. The decrease of the excess layer density from monolayer to bilayer is expected from the increase of the average coordination in the bilayer on the basis of the effective-medium theory [20] and from the decrease of the substrate attraction as the film thickness increases [21]. It is interesting to note that Tl does not form bilayers on gold (111) and (100) surfaces, although it has nearly identical monolayer structures as that on silver (111) and (100) surfaces.

3.4. Structure of bulk deposits

Layer-by-layer growth can be achieved (up to two layers) by controlling the potential in the UPD potential region. This is not the case at potentials negative of the Nernst potential, where bulk deposition starts. In the UPD region Tl atoms are deposited because they bind stronger to the substrate atoms than to the atoms of their own species. Deposition occurs, therefore, under equilibrium conditions and growth of well-defined monolayers or bilayers can easily be achieved. Further deposition onto the bilayer requires a potential negative of the Nernst potential (cf. Fig. 1) which results in a continuous multilayer growth. The growth mode is now under kinetic control and may vary with the potential and the Tl^+ concentration. Due to the thin layer geometry of the X-ray experiment, kinetic parameters are difficult to control, which imposes substantial difficulties on in situ studies of the growth mode. Instead our discussion is focused on the structure of the deposit.

The first SXS measurement for bulk deposits was carried out on a Tl thin film deposited at -0.53 V, about 60 mV below the Nernst potential, with the cell inflated. From the measured charge we estimate the amount of Tl deposited on the surface is a few hundred nominal atomic layers. After deflating, further deposition on the crystal surface was strongly limited by the slow transport of Tl^+ ions through the thin solution layer. The

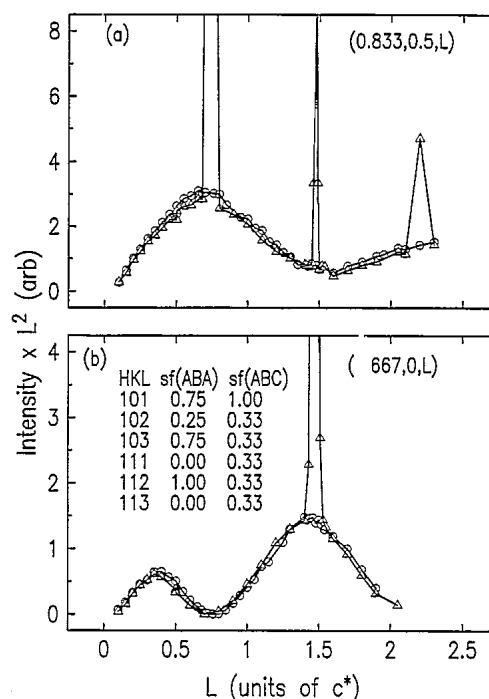


Fig. 6. Surface rods measured at -0.47 V for the $c(1.2 \times 2)$ bilayer (circles) and at -0.53 V for the $c(1.2 \times 2)$ bilayer plus hcp multilayers (triangles). The solid lines are for guiding the eyes. The (10) and (11) Tl rods are measured at (0.833, 0.5) and (1.667, 0) in-plane positions of the substrate coordinate, respectively. The inset of (b) lists the calculated structure factors for AB and ABC stacking sequences of Tl multilayer at six Bragg positions.

surface rod measurements were carried out at the deposition potential. As shown in Fig. 6, several very sharp and intense peaks appear in the two surface rods. These equally spaced spikes along the L direction are indicative of the formation of well-ordered three-dimensional crystallites. Despite the presence of these spikes, the intensity at all other positions are nearly the same as the ones measured at -0.47 V (circles) for the Tl bilayer.

One possible explanation for the constant intensity in the bilayer rods (discussed above) is that the bulk crystallites only cover a small region of the crystal. In order to test this idea, extended bulk deposition was carried out at -0.58 V. While the intensity of the spikes increased by about five times, there is no decrease of intensity at all other positions. These facts indicate that the commensurate $c(1.2 \times 2)$ bilayer is stable in the presence of bulk deposits on top of it. In contrast, a previous

SXS study on deposition of Pb on Ag(111) had shown that the diffraction signal from the compressed UPD monolayer vanishes as it restructures after an overpotential deposition of five nominal lead layers [5]. To rule out kinematic hindrance as the reason for the stability of the Tl $c(1.2 \times 2)$ structure, SXS measurements were also carried out with an overpotential deposition on the monolayer. The surface rods measured after a single step change of the potential from the monolayer to the bulk deposition potential region show the same feature as in Fig. 6. The fact that the same bilayer structure forms during this multilayer deposition process indicates that the existence of the biatomic-thick $c(1.2 \times 2)$ interlayer between the bulk phase and the substrate is the consequence of minimization of the interface energy and in-plane lattice strains. A more detailed discussion on the interlayer structure and its effect on the ordering of the bulk deposits and a comparison with other systems will be given in the next subsection.

Accurate measurements on the in-plane structure of the bulk deposit were carried out at $L = 1.476$ and 0.738 , corresponding to the sharp peaks in the $(0.833, 0.5)$ surface rod (cf. Fig. 6a), where the interference from the bilayer is minimal. The in-plane peak position was found at $(0.839, 0.484)$ which indicates that the bulk crystallites are incommensurate with the bilayer along both H and K directions. Additional diffraction peaks were found for every 30° sample rotations while keeping the same radial length ($\sqrt{(0.839^2 + 0.484^2)} = 0.9686$). Thus the bulk deposit forms an incommensurate hexagonal structure with respect to the underlying bilayer. Because the diffractions are at $0, 30,$ and 60 degrees from the substrate axes, the hexagonal structure has two symmetry-equivalent domains which are aligned exactly along each of the substrate axes. The hexagonal lattice constant was thus calculated to be 3.444 \AA which is slightly smaller (by 0.3%) than the hexagonal spacing of 3.456 \AA in bulk hcp Tl. The azimuthal scan width is 0.11° HWHM at $(0.839, 0.484, 0.738)$ which indicates that the mosaic spread of the Tl bulk deposit is as good as that of the Ag(100) substrate. The peak width in H and K scans are about 0.005 \AA^{-1} HWHM giving a coherence length of 200 \AA .

From the observed Bragg peaks, the three-dimensional structure of the bulk Tl crystallites can be derived. Two stacking sequences (ABA or ABC) are possible for the bulk hexagonal layers because there are two three-fold hollow sites per unit cell. The calculated structure factors at six low-order Bragg positions for the ABA and ABC stacking sequences are listed in the inset of Fig. 6b. For both stacking sequences, all the Bragg diffractions in the (10) Tl rod have nonzero structure factors which is consistent with the observation of all three corresponding peaks in Fig. 6a. The absence of diffraction peak at $(1.667, 0, 0.738)$ (see Fig. 6b), which corresponds to the (111) Bragg position in the (11) Tl rod, is expected by the structure factor calculation for the ABA but not the ABC stacking sequence. Therefore, it is evident that the Tl crystallites have the same hcp structure as its bulk crystal at room temperature.

Two typical L scans through the $(0.839, 0.484, 0.738)$ and $(0.839, 0.484, 1.476)$ peaks are shown in Figs. 7a and 7b. The data are better represented by a Gaussian than a Lorentzian line shape which is often the case for a multilayer. The average coherence length along the surface normal direction is at least 70 \AA , calculated from the HWHM ($0.009c^*$) of the $(0.839, 0.484, 1.476)$ peak, which corresponds to 25 Tl layers. The layer spacing calculated from $4.086/1.476$ is 2.768 \AA which is slightly larger (0.2%) than the bulk value of 2.763 \AA . Therefore, the Tl crystallites appear to compress within the surface plane and expand

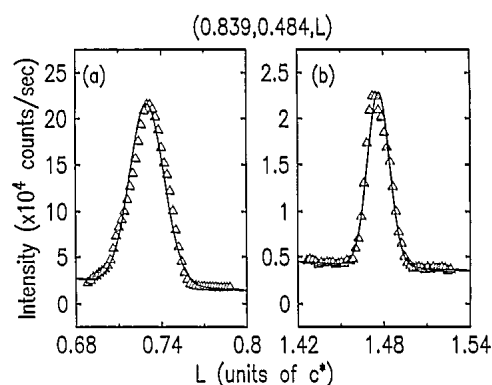


Fig. 7. L scans through two Bragg reflections of the hcp-Tl multilayer at -0.53 V . The solid lines are the fits to a Gaussian line shape.

along the surface normal compared to its free bulk crystal in a small amount. However, more detailed measurements are required to confirm the reproducibility and accuracy of these lattice parameters.

3.5. Structure of the hcp-Tl/Ag(100) interface

In this section, structural results on the electro-deposition of Tl on the Ag(100) surface are summarized and compared with data on Au(100). The comparison provides insight on the structure-determining factors in heteroepitaxy. The Tl layer density, normalized to the bulk Tl value, is shown in Fig. 8a and the lattice angle of the primitive unit cell (i.e., the angle between A and B in Fig. 2b) is shown in Fig. 8b. As discussed below, these figures summarize the potential dependent compression and distortion of the overlayers and the lattice mismatch at the interfaces.

Fig. 8a shows that the $c(p \times 2)$ Tl monolayer on the Au(100) and Ag(100) surfaces achieves the same maximum layer density (6% higher than the bulk) as do the hexagonal Tl monolayers on Ag(111) and Au(111) surfaces [10]. This identical excess layer density indicates a similar compress-

ive strain in all four monolayer phases. It can be explained by the reduced coordination at a surface in the framework of effective-medium theory [20] (see Section 3.3).

In contrast to the hexagonal monolayers on the (111) surfaces, the $c(p \times 2)$ adlayer lattices on the (100) surfaces are slightly distorted from a perfect hexagonal symmetry. This is manifested by the angle between the primitive cell vectors which slightly differs from the hexagonal value of 120° (cf. Fig. 8b) and the difference in the lengths of the primitive vectors (cf. Fig. 3b). The strain energy associated with this symmetry distortion is small and can be easily compensated by the reduction of the interface energy (i.e. the adsorbate-substrate interaction energy). The interface energy, which is given by summing over the adsorption energies of all the individual adatoms, depends on where the adatoms reside on the substrate lattice sites. When the adlayer is pseudomorphic to the substrate, the interface energy is the lowest since all the adatoms can occupy the lowest energy (“hollow”) sites. For an incommensurate adlayer, the high energy (“atop”) sites cannot be completely avoided giving rise to a higher interface energy. The energy difference between the “hollow” and “atop” sites increases as the surface corrugation increases. As a result, many monolayers form incommensurate hexagonal structures on the least corrugated (111) surfaces, but not on the more corrugated (100) and (110) surfaces. It is evident from the real space models in Fig. 4 that all the Tl adatoms in the uniaxially commensurate $c(p \times 2)$ phase reside between the rails of the (100) substrate atoms. Thus, the high energy “atop” sites are not occupied and the interface energy is significantly lower compared to an incommensurate monolayer.

The restructuring of the Tl monolayer on Ag(100) upon deposition of additional layers and the stability of the bilayer structure in the presence of the bulk Tl phase can be understood following arguments similar to those given above. In the former case, the restructuring occurs only along the incommensurate direction and leads to a high-order commensuration. Hence, the interface energy does not increase. Conversely, a restructuring of the $c(1.2 \times 2)$ bilayer to an incommensurate hexagonal lattice would require a large increase of the

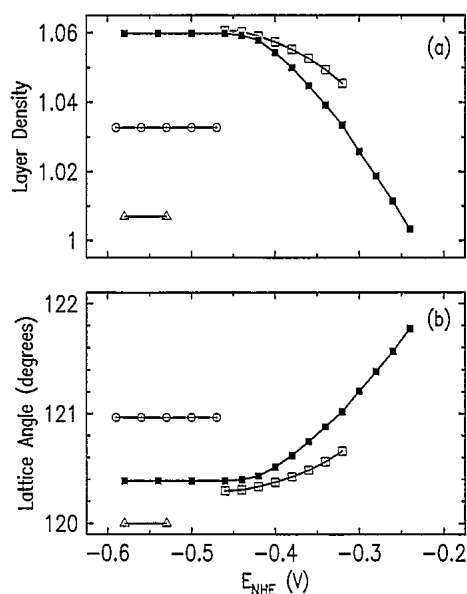


Fig. 8. (a) Tl layer density normalized to the hcp-Tl bulk value and (b) lattice angle of the in-plane unit cell for Tl monolayer (squares), bilayer (circles), and multilayer (triangles) as a function of potential. The data for the Tl monolayer on Au(100) are given by the solid squares for comparison.

interface energy since some adatoms have to occupy “atop” sites in the latter phase. On the other hand, the interface energy between the $c(1.2 \times 2)$ bilayer and the hcp bulk phase is small since the $c(1.2 \times 2)$ structure is only slightly distorted from hexagonal close-packing and is much less corrugated than the Ag(100) substrate. Therefore, the restructuring of the $c(1.2 \times 2)$ bilayer is energetically unfavorable.

The $c(p \times 2)$ uniaxially commensurate Tl monolayer on Au(100) also retains its structure after bulk deposition which supports the explanation based on the large interface-energy deduction resulting from uniaxial commensuration on corrugated (100) surfaces. The thickness of the interlayer (monolayer or bilayer) is different for the two surfaces because it depends on the way that the substrate–adatom interaction decays along the surface normal direction. Whereas bulk Tl deposits form hcp crystallites on both Au(100) and Ag(100) surfaces, the diffraction features are significantly weaker and broader on Au(100). This can be attributed to the higher excess layer density of the Tl interlayer on Au(100) compared to that on Ag(100) (cf. Fig. 8a). The larger lattice mismatch between the single interlayer and the bulk lattice causes a larger interface energy and in turn a less perfect bulk crystallites.

Further comparison of interface structures can be made with the Pb/Ag(111) system in which the deposition of bulk Pb causes the UPD monolayer structure to vanish. It is known that Pb and Tl both form incommensurate, hexagonal monolayers on Ag and Au (111) surfaces with nearly identical excess layer densities at the most negative potentials [10]. The reason for comparing with Pb/Ag(111) is the availability of the data on bulk deposition. Because of the small corrugation of the (111) surface and the incommensuration of both the Pb monolayer and the bulk phase with the Ag(111) substrate, the interface energy for the Pb monolayer on Ag(111) can be only slightly lower than that for the bulk Pb on Ag(111). The monolayer, therefore, restructures to the bulk phase because formation of an additional interface between the monolayer and the bulk phases would cost extra energy. The bulk Pb gives rise to a weak diffraction in the in-plane radial scans and no peak

in azimuthal scans. This indicates that the Pb islands, with its fcc-(111) texture, are randomly oriented on the substrate surface. For the three systems discussed, the crystalline perfection in bulk phase decreases in the order: Tl/Ag(100), Tl/Au(100), and Pb/Ag(111). This can be attributed to the increase of the lattice mismatch between the bulk deposit and the underlying substrate. These results demonstrate the pronounced effect of the interfacial atomic structure in determining the crystalline quality of the bulk deposits.

4. Conclusions

The above results demonstrate that SXS is particularly suitable for providing detailed and accurate structural information in under- and over-potential metal depositions on single crystal surfaces due to its high resolution and three-dimensional capability. Three distinct in-plane structures have been determined for Tl overlayers on Ag(100) as the film grows from a monolayer to a bilayer, and to multilayer deposits. The influence of the substrate–adatom interaction on the bilayer formation is demonstrated in a comparison with the deposition of Tl on Au(100). The stability of the bilayer structure in the presence of bulk deposits and its pronounced effects on subsequent epitaxial growth are explained in terms of strain and interface energies.

Acknowledgements

This research was performed under the auspices of the US Department of Energy, Divisions of Chemical and Materials Sciences, office of Basic Energy Sciences under Contract No. DE-AC02-76CH00016. We would like to thank Mike Weinert for valuable discussions.

References

- [1] J.H. van der Merwe, in: *Chemistry and Physics of Solid Surfaces*, Vol. 2, Ed. R. Vanselow (CRC Press, Boca Raton, FL, 1979) p. 129.

- [2] R.R. Adzic, J. Wang, C.M. Vitus and B.M. Ocko, Surf. Sci. 293 (1993) L876.
- [3] J.X. Wang, R.R. Adzic, O.M. Magnussen and B.M. Ocko, Surf. Sci. 335 (1995) 120.
- [4] (a) M.G. Samant, M.F. Toney, G.L. Borges, L. Blum and O.R. Melroy, Surf. Sci. 193 (1988) L29;
(b) O.R. Melroy, M.F. Toney, G.L. Borges, M.G. Samant, J.B. Kortright, P.N. Ross and L. Blum, Phys. Rev. B 38 (1988) 10962.
- [5] O.R. Melroy, M.F. Toney, G.L. Borges, M.G. Samant, J.B. Kortright, P.N. Ross and L. Blum, J. Electroanal. Chem. 258 (1989) 403.
- [6] (a) M.F. Toney, J.G. Gordon, G.L. Borges, O.R. Melroy, M.G. Samant, D. Wiesler, D. Yee and L.B. Sorensen, Phys. Rev. B 42 (1990) 5594;
(b) M.F. Toney, J.G. Gordon, M.G. Samant, G.L. Borges, O.R. Melroy, D. Yee and L.B. Sorensen, Phys. Rev. B 45 (1992) 9362.
- [7] (a) J.X. Wang, R.R. Adzic and B.M. Ocko, J. Phys. Chem. 98 (1994) 7182;
(b) W. Polewska, J.X. Wang, B.M. Ocko and R.R. Adzic, J. Electroanal. Chem. 376 (1994) 41.
- [8] (a) B.M. Ocko, G.M. Gavin and J. Wang, J. Phys. Chem. 98 (1994) 897;
(b) O.M. Magnussen, B.M. Ocko, R.R. Adzic and J.X. Wang, Phys. Rev. B 51 (1995) 5510.
- [9] (a) O.M. Magnussen, J. Hotlos, G. Beitel, D.M. Kolb and R.J. Behm, J. Vac. Sci Technol. B 9 (1991) 969;
(b) O.M. Magnussen, J. Hotlos, R.J. Nichols, D.M. Kolb and R.J. Behm, Phys. Rev. Lett. 64 (1990) 2929;
(c) S. Manne, P.K. Hansma, J. Massie, V.B. Elings and A.A. Gewirth, Science 251 (1991) 183.
- [10] M.F. Toney, J.G. Gordon, M.G. Samant, G.L. Borges, O.R. Melroy, D. Yee and L.B. Sorensen, J. Phys. Chem. 99 (1995) 4733.
- [11] The reference point for the strain in an adsorbed monolayer is not unique. For example, the adlayer strain could, in theory, be related to a free-standing monolayer or to a monolayer on top of a “jellium” substrate. For the present study of the structural evolution from monolayer to bulk, however, the bulk lattice is the natural reference.
- [12] (a) P.M. Marcus and F. Jona, Phys. Rev. B 51 (1995) 5263;
(b) H. Brune, H. Roder, C. Boragno and K. Kern, Phys. Rev. B 49 (1994) 49;
(c) R. Bruinsma and A. Zangwill, J. Physique 47 (1986) 2055;
(d) S. Stoyanov, Surf. Sci. 172 (1986) 198.
- [13] C. Gunther, J. Vijmoeth, R.Q. Hwang and R.J. Behm, Phys. Rev. Lett. 74 (1995) 754.
- [14] H. Siegenthaler, K. Juttner, E. Schmidt and W.J. Lorenz, Electrochim. Acta 23 (1978) 1009.
- [15] (a) G. Staikov, E. Budevski, M. Hopfner, W. Obretenov, K. Juttner and W.J. Lorenz, Surf. Sci. 248 (1991) 234;
(b) W. Obretenov, U. Schmidt and W.J. Lorenz, G. Staikov, E. Budevski, D. Carnal, U. Muller, H. Siegenthaler and E. Schmidt, J. Electrochem. Soc. 140 (1993) 692.
- [16] (a) A. Hamelin, L. Stoicoviciu, L. Doubova and S. Trasatti, J. Electroanal. Chem. 244 (1988) 133;
(b) T. Kurasawa, Patent Japan, 35–5619, 23 May 1960.
- [17] J. Wang, B.M. Ocko, A.J. Davenport and H.S. Isaacs, Phys. Rev. B 46 (1992) 10321.
- [18] The bonding energies between metal adatoms and different metal substrates are known to increase as the difference in work functions of substrate and adsorbate increases [19]. Gold has higher work function than silver, hence it interacts stronger with Tl, Pb, and Bi adatoms than Ag. This is consistent with the facts that larger UPD potential ranges were observed on Au than on Ag in most of the cases.
- [19] D.M. Kolb, M. Przasnyski and H. Gerischer, Electroanal. Chem. Interfac. Electrochem. 54 (1974) 25.
- [20] K.W. Jacobsen, J.K. Nørskov and M.J. Puska, Phys. Rev. B 35 (1986) 7423.
- [21] (a) G. Staikov, E. Budevski, W. Obretenov and W.J. Lorenz, J. Electroanal. Chem. 349 (1993) 355;
(b) J. Villain and M.B. Gordon, Surf. Sci. 125 (1983) 1.